Development of a Generic Three-Dimensional Finite Element Fibre Pullout Model

Mohammad Hajsadeghi [a,b*], Chee Seong Chin [b], Stephen W. Jones [a]

[a] *School of Engineering, University of Liverpool, Liverpool L69 3BX, UK*

[b] *Department of Civil Engineering, Xian Jiaotong-Liverpool University, Suzhou Industrial Park, Jiangsu Province, China*

ABSTRACT:

Considering the relative advantages of Finite Element (FE) simulation compared with physical tests and analytical methods, in this paper a generic nonlinear FE model for steel fibres pullout from cementitious matrix is presented. In the model, cohesion, interfacial debonding, sliding frictional contact, fibre deformation, and material plasticity are incorporate.

The complete bond-slip response of the proposed model is validated using experimental results obtained from the literature. Finally, the validated pullout model is employed as a virtual laboratory unit to investigate the pullout performance of two new steel fibres and optimise the fibres material.

Keywords: nonlinear finite element simulation; fibre pullout mechanism; cementitious composite; steel fibre design.

Highlights:

- A generic nonlinear finite element model for steel fibres pullout from concrete is proposed.
- In the model, cohesion, interfacial debonding, frictional sliding, fibre deformations, and material plasticity are incorporated.
- Good agreement between the experimental and numerical results is achieved.
- The validated model is employed as a virtual laboratory unit to design new steel fibres.

GRAPHICAL ABSTRACT:

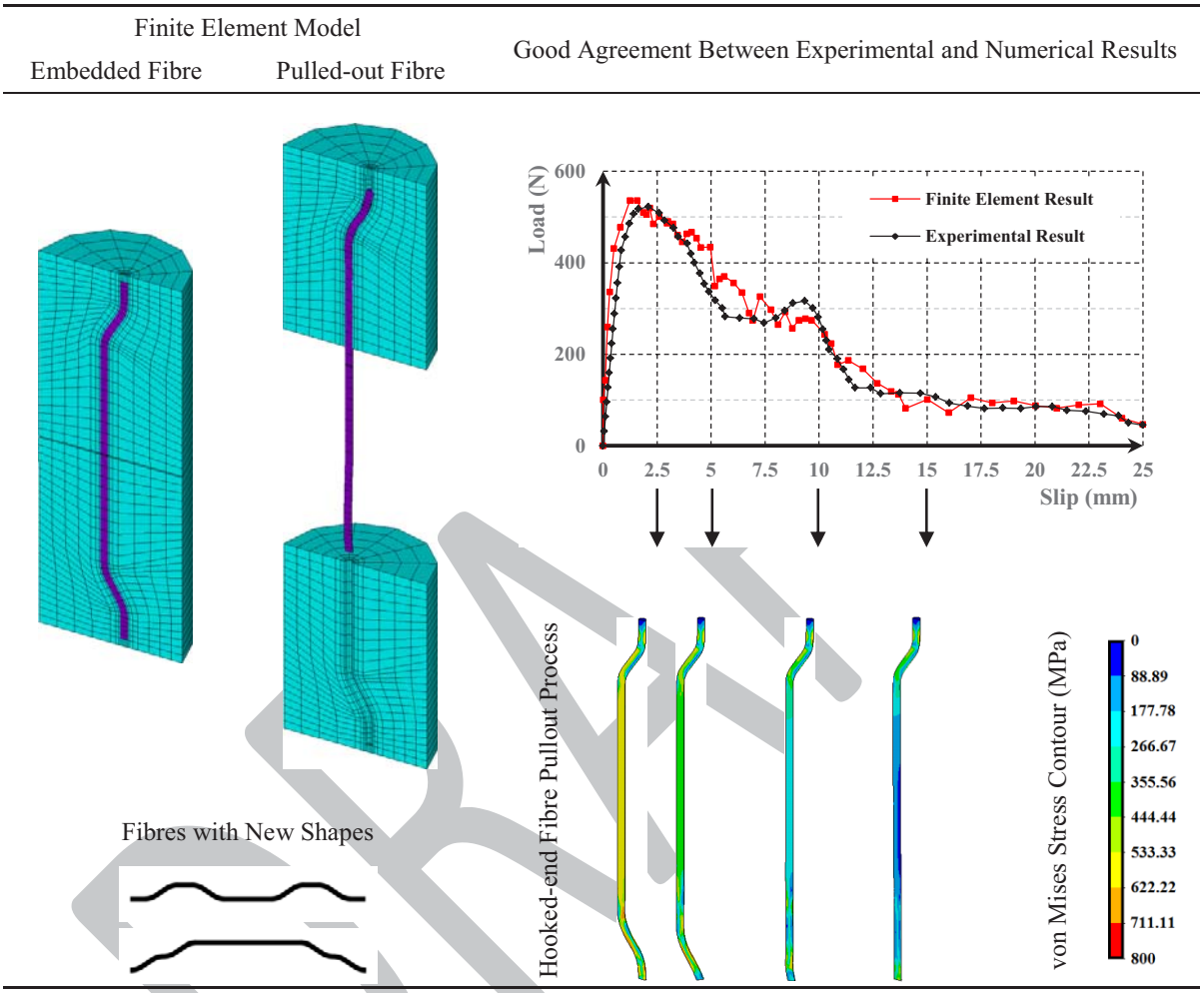

NOTATIONS

c	Contact cohesion, MPa;
d	Decay coefficient;
E_c	Young's modulus of concrete, GPa;
E_s	Young's modulus of steel, GPa;
E_t	Total dissipated pullout energy, Nm;
f_{ck}	Characteristic cylinder strength of concrete, MPa;
f_{ctm}	Mean tensile strength of concrete, MPa;
f_n	Normal component of contact force, N;
f_t	Tangential component of contact force, N;
f_u	Ultimate stress of steel, MPa;
f_y	Yield stress of steel, MPa;
F	Force vector;
g_n	Penetration along the normal direction, mm;
g_t	Penetration along the tangential direction, mm;
k_n	Normal penalty stiffness, N/mm;
k_t	Tangential penalty stiffness, N/mm;
K_b	Stiffness matrix of the contacting bodies;
K_c	Contact stiffness matrix;
l_{em}	Embedded length, mm;
P_{max}	Maximum pullout load, N;
u	Displacement vector;
ε_u	Ultimate strain of steel;
μ	Frictional coefficient;
μ_d	Dynamic coefficient of friction;
μ_s	Static coefficient of friction;
v	Slip rate, mm;
v_c	The Poisson's ratio of the concrete;
v_s	The Poisson's ratio of the steel;
ρ	Normal contact pressure, MPa;
τ	Equivalent shear stress, MPa;
τ_{max}	Maximum shear stress, MPa;

1. INTRODUCTION

The main disadvantage of concrete under low confining pressure is its brittleness, i.e., relatively low tensile strength and ductility and poor resistance to crack opening and propagation. Therefore once cracking is initiated, concrete drastically loses its load carrying capacity in tension. This drawback which limits practical applications of plain concrete could be overcome by the inclusion of a small amount of discontinuous and short steel fibres which are randomly distributed within the concrete. This composite material is generally known as Fibre Reinforced Concrete (FRC) [1,2].

Among all the common fibre materials, steel is the most suitable for structural purposes [1]. In the early days of Steel Fibre Reinforced Concrete (SFRC), the fibres were mostly undeformed (straight) [3]. The crack bridging performance of such fibres directly depends on the physical and chemical adhesions between the fibres and the surrounding matrix (physicochemical bond) which are predominantly determined by the properties of the fibre-matrix interface and matrix packing density [4]. More recent research indicates that the mechanical anchorage in the deformed fibres effectively improves pullout resistance [3,5,6]. The mechanical bond properties are determined by the physical geometry of the fibre and the transverse tensile strength of the matrix. The mechanical anchorage could be provided by deformation at the fibre ends, such as with hooked-end fibres (which locally increases the mechanical bond), or deformation along the fibre length, such as in crimped or twisted fibres (which provides a mechanical bond along the fibres) [4]. Typical steel fibres are shown in **Fig. 1**.

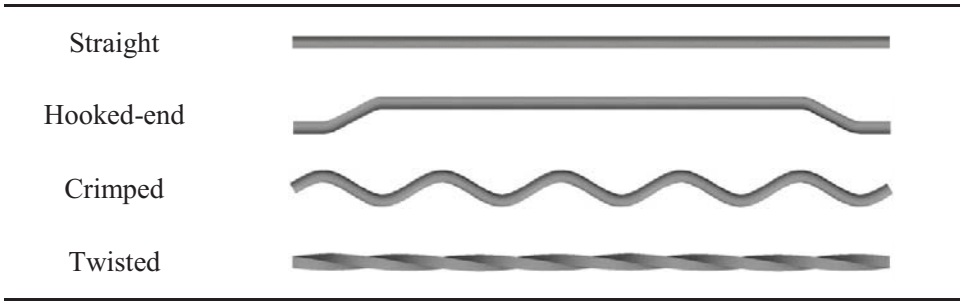

Fig. 1. Types of steel fibre.

The evaluation of post-cracking response has main importance for SFRC composites to be effectively and economically employed in practice. The residual post-cracking tensile strength of conventional SFRC is directly related to both fibre volume content (specifically the amount of fibres crossing a crack) and the fibre-matrix interfacial bond characteristics. Although such characteristics are best described by a bond-shear-stress-slip relationship, the direct experimental determination of such a relationship has not yet been possible. However, a load versus slip response which can be obtained from the fibre pullout test is employed by researchers to study the characteristics of the fibre-matrix interface [7-9].

The structural contribution of such material mainly depends on its tensile/flexural characterisation. Currently there is no standard direct tension test for fibrous concrete mainly because it is difficult to provide a proper gripping arrangement to avoid specimen cracking at grips. On the other hand, bending test is a widely used test method for performance evaluation of SFRC [10].

Analytical procedures can be employed to correlate the pullout response of individual fibres with the overall direct tensile and flexural performances of SFRC specimens where the fibre inclination, embedment length, and fibre density distribution are taken into account [11,12]. For instance, Armelin and Banthia [11] developed a model based on simple principles of mechanics to estimate the flexural response of SFRC prisms. The pullout load-slip relationship of single

fibres at different angles of inclination and the compressive strength of the matrix are the input parameters of the model. Furthermore, there are closed-form formulations presented in the literature to back-calculate constitutive material behaviours in compression and tension from flexural test result. The constitutive material models are required in the design of structural members [13-15].

Therefore, the knowledge of the single fibre pullout behaviour is essential to understand the uniaxial or bending behaviour of SFRC composites.

The fibre-bridging-pullout process is a sophisticated mechanism which consists of cohesion, interfacial debonding, sliding frictional contact, fibre deformation and material plasticity. Since the introduction of steel fibre, numerous research studies have been conducted to investigate the pullout mechanism of such fibres interacting with concrete. However, limited research has been carried out using Finite Element (FE) and analytical methods, while the majority of the investigations were conducted experimentally [3,4,6-9,16-19].

An analytical model of the entire pullout process for smooth steel fibres was developed by Naaman et al. [18] where a bond-stress-slip relationship of the interface with decaying behaviour capability was incorporated in the model to capture the descending branch of the pullout response. The effect of hook deformation as the mechanical anchorage on the pullout mechanism of steel fibres was advanced by Van Gysel [20,21] using the principle of energy conservation. The investigation was based both on theoretical and experimental considerations where fibre debonding, plastic deformation, and additional frictional force due to incomplete straightening of the hook was taken into account. Alwan et al. [22] presented an alternative approach using the concept of the frictional pulley to simulate the hook action. The model consists of two frictional pulleys which have rotational and tangential components of friction resisting the pullout process.

The components respectively correspond to the work required for the fibre straightening and friction between the fibre and matrix in the curved duct. Sujivorakul et al. [23] employed the concept of nonlinear springs to simulate the effect of the hook. The approach superposes the effect of the spring on the previously proposed pullout models for straight fibres by applying an iterative procedure over the geometry of the mechanical anchorage. A model to predict the pullout of mechanically deformed steel fibres from concrete was developed by Zīle and Zīle [9] based on the law of conservation of energy. The increase in the pullout load caused by mechanical anchorage depends on the amount of plastic work required to straighten the fibre during pullout. The model predictions were compared with experimental pullout results of the hooked-end and crimped steel fibres where good agreement was observed.

In addition, there are other analytical investigations focused on the pullout behaviour of fibres embedded in concrete with varying inclinations respect to the loading direction. In this case, the fibre-matrix interaction at the point where fibre exits the matrix, i.e. exit point of fibre, becomes highly complex. These pullout scenarios better represent the ones existing in practical applications, where random orientation of fibres is likely to occur. Laranjeira et al. [24] presented an analytical model to predict the pullout response of straight steel fibres embedded in concrete with varying angles of inclination. A model to predict the pullout response of inclined hooked-end steel fibres was developed by Laranjeira et al. [25]. The model is based on the fibre geometry, strength of the fibre and matrix materials, and experimental data of fibres aligned with the load direction. The fibre-matrix interaction at the exit point is considered by estimating the amount of spalled matrix and by including local friction effects.

The analytical models developed are applicable for specific cases of pullout problems. In the case of complex geometries and/or boundary conditions, many approximations and simplifying

assumptions must be made which could lead to an inaccurate prediction of the pullout performance. In most cases, FE simulation is more economic and faster than conducting physical tests. Moreover, with the current level of technology, the details which could be obtained from the simulations are significantly higher than those of the tests. Therefore, the establishment of a generic nonlinear FE model to simulate the mechanism of fibre pullout from the concrete matrix is an instructive solution to tackle such a problem.

Two-dimensional (2D) FE models for the fibre pullout mechanism were adopted by several researchers [26-28]. Tsai et al. [26] proposed a 2D finite element model based on an updated Lagrangian formulation to simulate a quasi-static pullout process of elastoplastic fibres. The nonlinear behaviour of the fibre-matrix interface was approximated using the combination of cohesive and Columb friction models. Li and Mobasher [27] presented a pullout model capable of simulating the stable debonding process. The failure condition of the interface was modelled using a biaxial yield surface and after debonding, a Coulomb frictional force was applied over the debonded interface. Yang et al. [28] presented a numerical simulation method to study the effect of the fibre embedment length and the matrix-wrapped thickness around the fibre on the behaviour of the fibre-matrix interface which was assumed to be bonded perfectly.

In addition, Georgiadi-Stefanidi et al. [29] proposed a three-dimensional (3D) FE pullout model for hooked-end fibres. The physicochemical bond of the fibre-matrix interface was taken into account by a number of nonlinear spring elements which transfer the bond stresses through a set of equivalent point loads. However, consideration of point loads rather than interfacial bond stresses is not accurate especially in the case of unsymmetrical and/or coarse mesh patterns at the interface. Introduction of additional elements, i.e. spring elements, would also increase the

solution time. Chin and Xiao [30], also, presented a 3D numerical model to capture complete pullout response of end- and fully-deformed steel fibres.

In this paper, a generic nonlinear 3D finite element model is proposed to analyse the complex bond-slip behaviour of fibres in concrete with various physical and geometrical properties. The numerical results are validated using experimental results obtained from the literature [4,6,9,31]. The validated model is then employed to investigate the pullout performance of two new shapes of steel fibre and optimise the fibres material. ANSYS is employed as a platform for all simulation tasks.

2. MODELLING OF THE STEEL FIBRE AND CEMENTITIOUS MATRIX

The 8-noded solid element with three degrees of freedom at each node (i.e. translations in the nodal x, y, and z directions) is used to model the steel fibres. The element has plasticity, stress stiffening, large deflection, and large strain capabilities. Cementitious matrices are modelled using the 8-noded solid brick elements with cracking, crushing and plastic deformation capabilities [32].

The von Mises yielding criterion is adopted to simulate the plasticity of the fibres material. The von Mises yielding criterion is combined with the modified Willam and Warnke failure criterion [33] to model the cementitious matrices.

The yield and ultimate stresses (f_y and f_u) and the ultimate strain (ε_u) for fibres material are taken from the actual experimental results. The modulus of elasticity and the Poisson's ratio of the steel material (E_s and υ_s) are taken as 210 GPa and 0.3 respectively. The uniaxial tensile and compressive strengths (f_{ctm} and f_{ck}) and the modulus of elasticity (E_c) of cementitious matrices are specified according to those experimentally obtained. However, in some cases where the actual tensile strength and the modulus of elasticity are not available, they are estimated using

Eqs. (1) and **(2)** in accordance with Eurocode 2 [34]. The Poisson's ratio of the cementitious material (υ_c) is taken as 0.2.

$$f_{ctm} = 0.3 \times f_{ck}^{2/3} \quad \text{(MPa)} \tag{1}$$

$$E_c = 22 \times \left(\frac{f_{ck} + 8}{10} \right)^{0.3} \quad \text{(GPa)} \tag{2}$$

3. THE FIBRE-MATRIX INTERFACE

The surface-to-surface contact is used to represent the contacting fibre and matrix surfaces (the fibre-matrix interface) which are respectively specified as contact and target surfaces. The contact and target elements have the same geometric characteristics overlaying the contacting surfaces which are capable of simulating the deformable contact interface.

The physicochemical bond of the fibre-matrix interface is defined by the Coulomb friction model where two contacting surfaces carry shear stresses up to a certain magnitude across their interface before they start sliding relative to each other. An equivalent shear stress (τ) is defined as a fraction of the normal contact pressure (ρ) at which sliding on the surface begins, as seen in **Eq. (3)** and **Fig. 2(a)**.

$$\tau = \mu \rho + c; \quad \tau \leq \tau_{max} \tag{3}$$

where μ is the coefficient of friction and c is the contact cohesion which provides sliding resistance even with zero normal pressure [35].

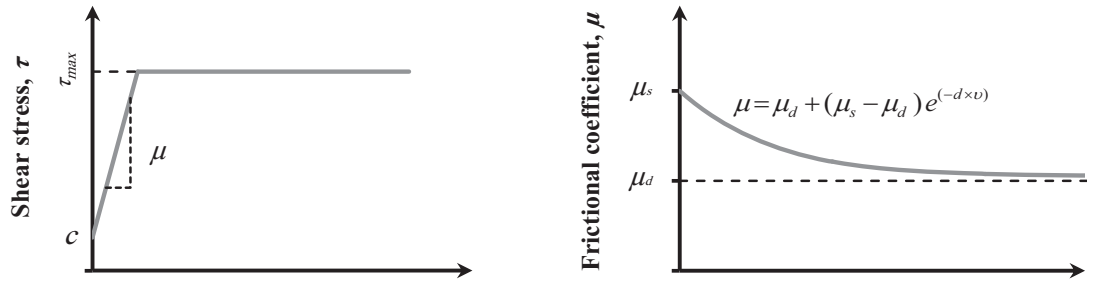

(a) Sliding contact resistance **(b)** Friction decay

Fig. 2. Properties of the fibre-matrix interface.

To consider interfacial debonding between the fibre and the surrounding matrix, the friction decay is specified based on **Eq. (4)** [36].

$$\mu = \mu_d + (\mu_s - \mu_d)e^{(-d\times\upsilon)} \qquad (4)$$

where μ_d and μ_s are the dynamic and static coefficients of friction, respectively, d is the decay coefficient, and υ represents slip rate (see **Fig. 2(b)**).

During the pullout process, material failure (mostly concrete) would occur at the high stress regions of the fibre-matrix interface. Therefore, the maximum contact friction, τ_{max}, is introduced in the friction model as seen in **Fig. 2(a)**, so that, irrespective of the magnitude of the normal contact pressure, sliding will occur once the frictional stress reaches this value [32]. The sticking/sliding calculations determine when a point transitions from sticking to sliding or vice versa.

The pure penalty method is employed to establish a relationship between the contact and target elements to prevent or limit penetration, i.e. contact compatibility, where the compatibility is

achieved using a fictitious spring. When contact is detected, the spring would deflect, thus creating an action (contact force) to resist the penetration. The spring stiffness is known as contact or penalty stiffness. The elements can transmit compressive normal and tangential forces but not tensile normal forces and they are free to separate and move away from each other [32,37-39].

Fig. 3 shows a contact scenario in which a contact element is penetrated into a target element. The contact element consists of a slave node and the target element is represented by a master line connecting nodes 1 and 2. S_o and S represent the slave node before and after penetration.

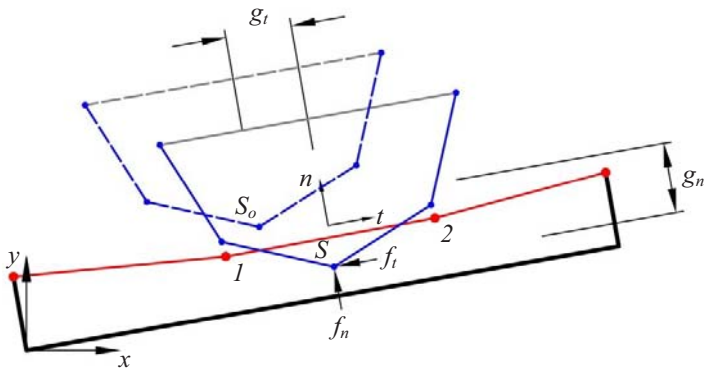

Fig. 3. Penalty method formulation.

The penetration is resisted by the contact force which is resolved into two components in the normal and tangential directions, i.e. f_n and f_f, and are defined by **Eqs. (5)** and **(6)** [31,37].

$$f_n = -k_n g_n \tag{5}$$

$$f_t = -k_t g_t \tag{6}$$

where g_n and g_t are penetrations along the normal and tangential directions and k_n and k_t are penalty terms which respectively express the relationship between the contact force and the penetration along the normal and tangential directions. Once the tangential contact force exceeds the static friction force, sliding will occur, as below.

$$\begin{aligned} f_t &< \mu_s f_n \quad \rightarrow \quad \text{Sticking State} \\ f_t &\geq \mu_s f_n \quad \rightarrow \quad \text{Sliding State} \end{aligned} \tag{7}$$

Considering the frictional contact problem produces non-symmetric stiffnesses, the unsymmetric solution is incorporated in the Newton-Raphson method to improve the computational efficiency [40-42].

As seen in **Fig. 4** and mentioned above, the contact and target elements overlay the surfaces of contacting bodies (the steel fibre and matrix) and have the same geometric characteristics as the underlying elements. Therefore, the compatibility is applied to the fibre and matrix surfaces which respectively underlay the contact and target elements.

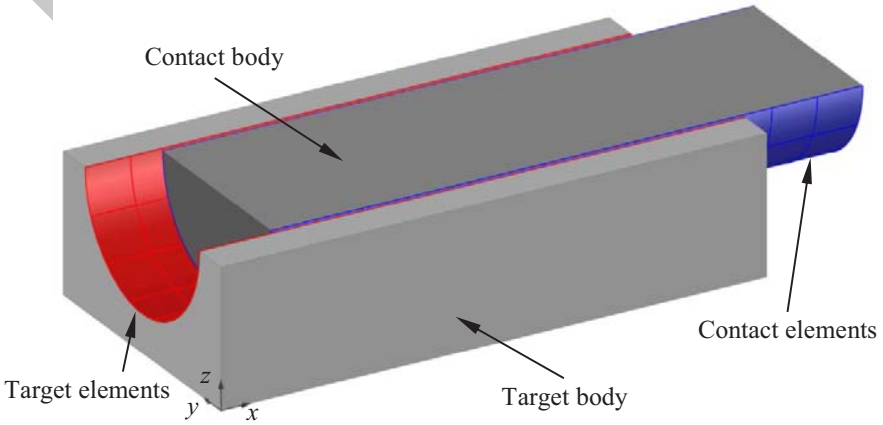

Fig. 4. Contact and target elements with corresponding bodies.

To derive the contact stiffness matrix, the contact surface is divided into a set of contact elements. The element represents the interaction between the surface nodes of the contact body with the corresponding element face of the target body. The contact stiffness matrix, K_c, is assembled into the stiffness matrix of the contacting bodies (K_b). The equilibrium equation for the system is expressed as **Eq. (9)**.

$$[K_b + K_c]u = F \tag{8}$$

where u and F are displacement and force vectors respectively [37,39].

The contact stiffness matrix depends on the contact status, whether the surfaces are touching or separated, therefore the matrix is a non-linear term [39]. In this study, the contact stiffness matrix is updated at each iteration. Ideally, zero penetration is only possible with an infinite contact stiffness which is numerically impossible with penalty-based methods. However, as long as the penetration value is in the allowable interpenetration range, the results are deemed to be valid. If the penetration is larger than the allowable value, i.e. penetration tolerance, the global solution would be invalid, even though the residual forces and displacements have met the convergence criteria [32].

In this research, asymmetric contact pair is selected for the contact modelling where the fibre and matrix surfaces are specified as contact and target surfaces respectively. Contact elements are constrained against penetration into the target surface at Gauss integration points as they generally provide more accurate results compared with nodal points (**Fig. 5**) [32].

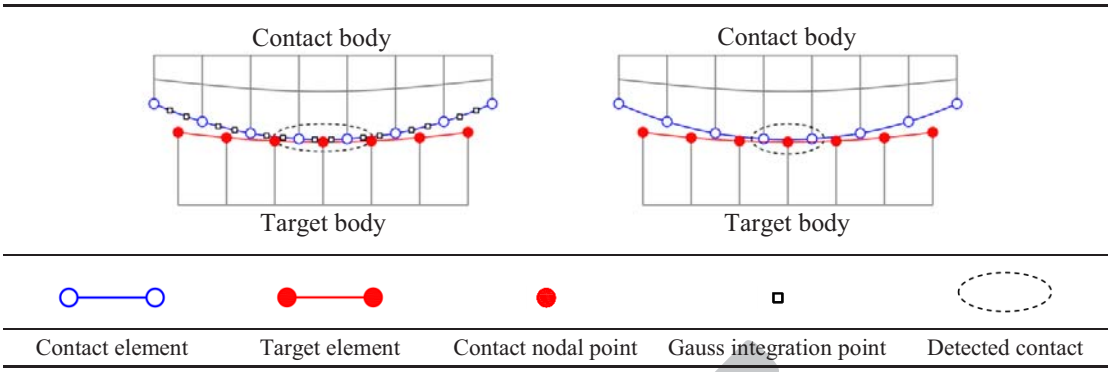

Fig. 5. Location of contact detection.

A spherical zone around each detection point of contact elements is used to determine far-field open and near-field open status known as the "Pinball Region". If a node on the target surface is within this sphere, it is considered to be in near contact and its relationship to the contact detection point is monitored more closely. The computational cost of searching for contact depends on the size of the pinball region [41]. The pinball region as a sphere of radius 2 times depth of the underlying elements of the contact surface is considered for all FE models.

In order to model debonding at the interface, two frictional coefficients, i.e. static and dynamic coefficients of friction, are introduced in the models. Therefore, before any slip occurs, the frictional force is calculated using the static coefficient (μ_s). After sliding happens, the interface friction is determined using **Eq. (4)** (see **Fig. 2(b)**). However according to **Eq. (3)**, the frictional stress, $\mu\ \rho$, is available just by the presence of normal contact pressure. Since at the beginning of the analysis, there is no normal pressure to activate static friction, an initial normal pressure on contact elements (the fibre surface at the interface) is required, before any slip occurs. To this end, the channel of the matrix surrounding the fibre is modelled with a diameter smaller than that of the fibre wire (in this study, the diameter of the channels is 0.05 mm smaller than that of the fibres). Then the model is analysed with the presence of initial penetration. Since the interpenetration is detected, the contact pressure is applied on the contact surface (fibre surface at

the interface) (see **Fig. 6**), to enforce the contact compatibility. Following applying the initial pressure, the incremental load is applied at the free end of the fibre in a displacement-controlled manner to capture the bond-slip response.

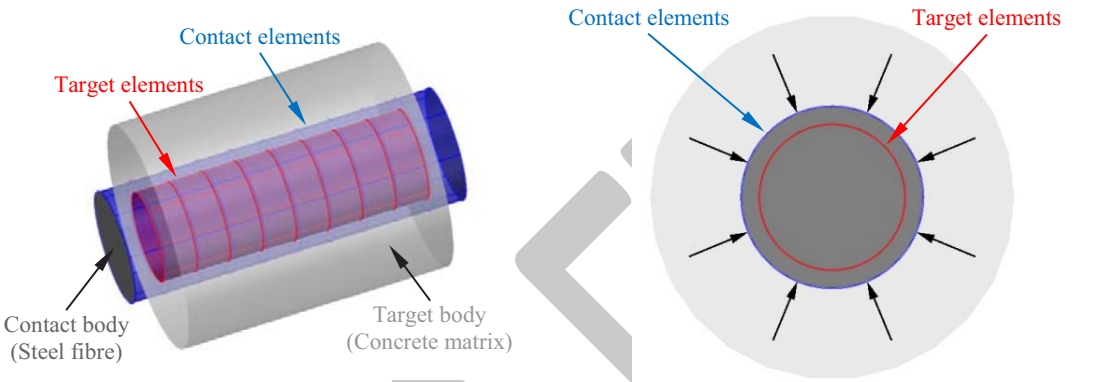

(a) Perspective view **(b)** Top view

Fig. 6. Applying initial contact pressure on the contact surface, i.e. steel fibre surface.

4. VALIDATION OF THE NUMERICAL MODEL

In order to define contact stiffnesses (normal and tangential) and penetration tolerance values, ANSYS provides two options, default and absolute values. Default values are determined based on the material properties and element size of the underlying elements of the contact surfaces as well as the frictional coefficients of the contact pair and the total number of degrees of freedom in the model. These default values can be modified in the contact pair (prior to the solution) by applying scaling factors. Furthermore, many factors may be applied (automatically by ANSYS) to the actual contact normal stiffness during the solution.

Throughout this study, absolute values are considered for contact stiffnesses and penetration tolerance (1500 N/mm and 0.01 mm, respectively); therefore contact stiffnesses are independent of the material properties and nonlinearity (such as steel plastification and concrete cracking),

and meshing pattern and size. However, during the pullout process, material failure would occur in the high-stress regions of the fibre-matrix interface. Hence, the maximum contact friction, τ_{max}, is introduced in the friction model (as seen in **Fig. 2(b)**) so irrespective of the magnitude of the normal contact pressure, sliding occurs once the frictional stress reaches this value.

Experimental pullout data of various steel fibres including straight, hooked-end, crimped, and twisted which were tested in the single-sided manner are employed to validate the proposed numerical model. Taking advantage of symmetry in geometry and loading of some specimens, a fraction of the specimens with consideration of proper boundary conditions are modelled. The contact parameters including μ_s, μ_d, c, d, and τ_{max} are determined for each model in accordance with the respective experimental data.

4.1. STRAIGHT STEEL FIBRE

Pullout testing data of a straight fibre given by Naaman and Najm [6] are employed for the validation. The geometrical and material properties of the fibre are provided in **Table 1**. The cylinder compressive strength of the cementitious matrix is 60 MPa. The mean tensile strength and Young's modulus of concrete are estimated to be 4.6 MPa and 39 GPa (**Eqs. (1)** and **(2)**). Due to symmetry in geometry and loading, a quarter of the specimen is modelled, as shown in **Fig. 7**. The contact parameters used for this model are presented in **Table 2**.

Table 1
Geometrical and material properties of the straight steel fibre, Naaman and Najm [6].

Cross-section	Diameter	Embedded length (l_{em})	Yield strength (f_y)	Ultimate strength (f_u)
Circular	0.48 mm	12.7 mm	450 MPa	600 MPa

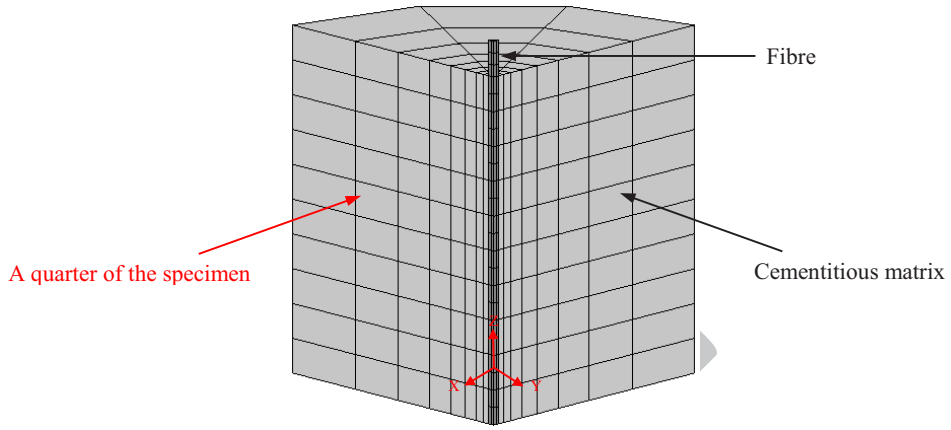

Fig. 7. Finite element model of the straight fibre.

Table 2
Considered contact parameters for the FE models.

Fibre type	Dynamic friction of coefficient	Static friction of coefficient	Cohesion (MPa)	Maximum contact friction (MPa)
	μ_d	μ_s	c	τ_{max}
Straight	0.32	2.82	4	80
Hooked-end	0.34	2.14	6	80
Crimped	0.30	2.42	5	80
Twisted	0.44 – 0.68 [a]	2.86	8	120

[a] The range of frictional coefficient.
* Decay coefficient (d) for all the models are considered to be 5.

Fig. 8 shows the comparison between the experimental and numerical bond-slip responses.

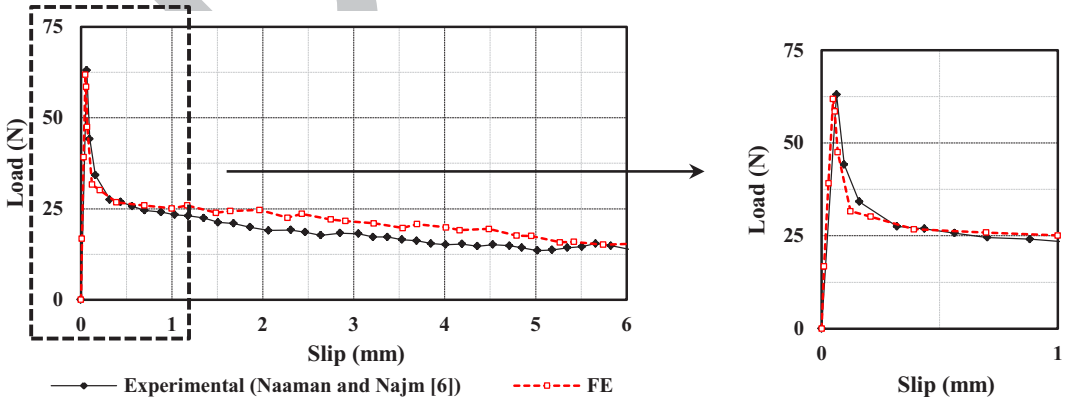

Fig. 8. Experimental and numerical load-slip curves of the straight fibre.

From the figure, the agreement between the experimental and numerical results is good and the model predicts the peak load as well as the pre-peak, debonding, and post-peak responses well. Average interfacial shear stresses (pullout loads divided by the corresponding fibre-matrix interface value) at various values of displacement along with the corresponding frictional contact stress (shear stress at the interface) contours are illustrated in **Fig. 9**. Agreement between the results is good which verifies a relatively constant shear stress at the interface after debonding [16].

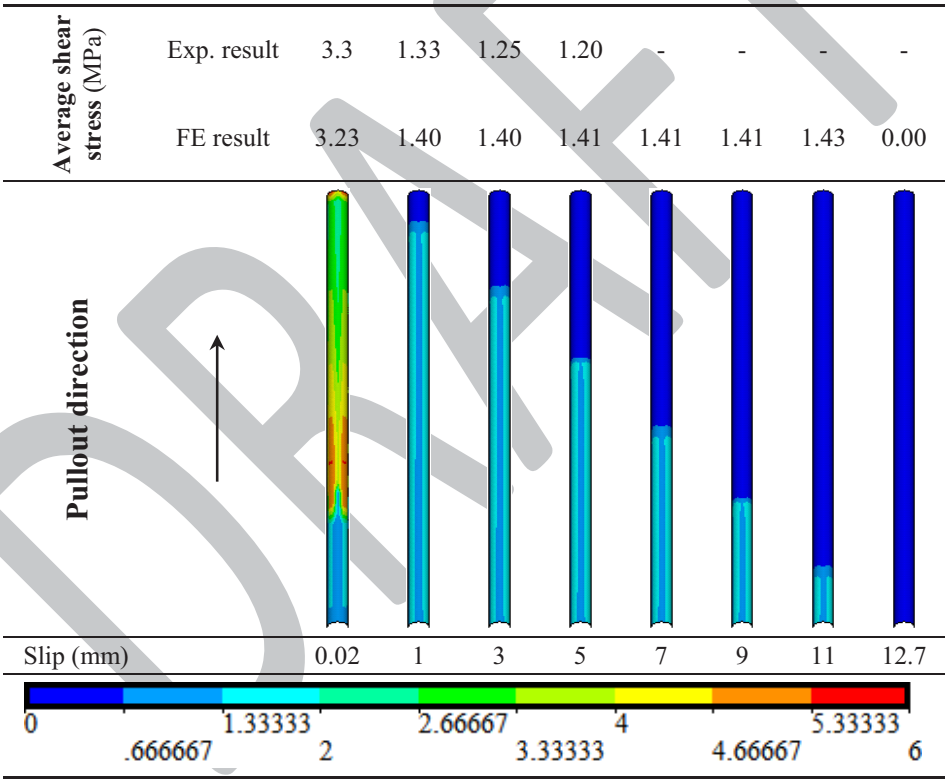

Fig. 9. The fibre-matrix interface of the straight fibre during pullout process.

Figs. 10(a) and **(b)** show the von Mises stress contours of the fibre at slips equal to 0.02 mm, corresponding to the maximum pullout load, and 2 mm. The normalised von Mises stress (with respect to the yield stress) at three levels along the fibre length (bottom, middle, and top of the

fibre) versus slip are illustrated in **Fig. 11**. The results indicate that the entire length of the fibre responds similarly to the pullout process by suffering considerable stress decay after the displacement corresponding to the debonding.

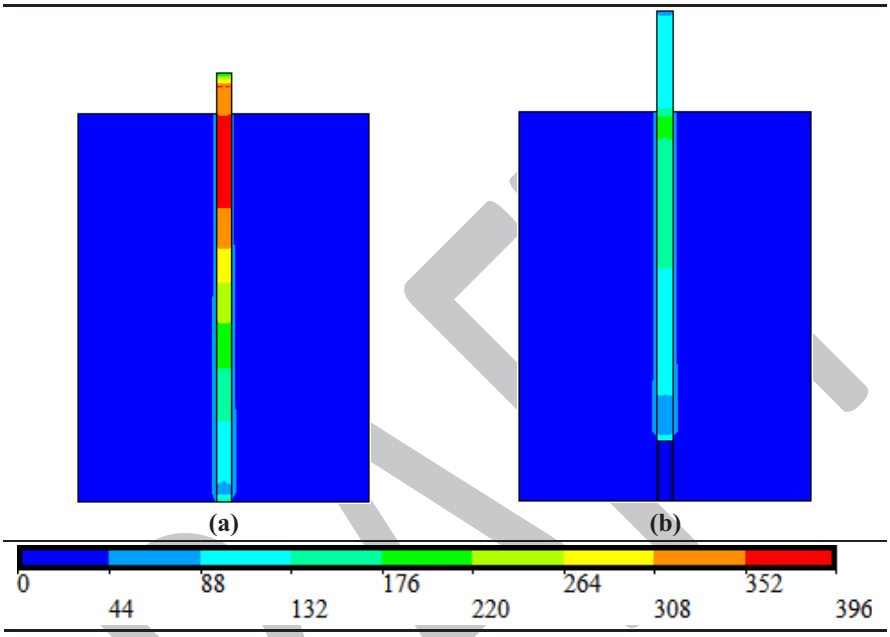

Fig. 10. The von Mises stress contours (in MPa) of the straight fibre at **(a)** slip = 0.02 mm, i.e. debonding; **(b)** slip = 2 mm.

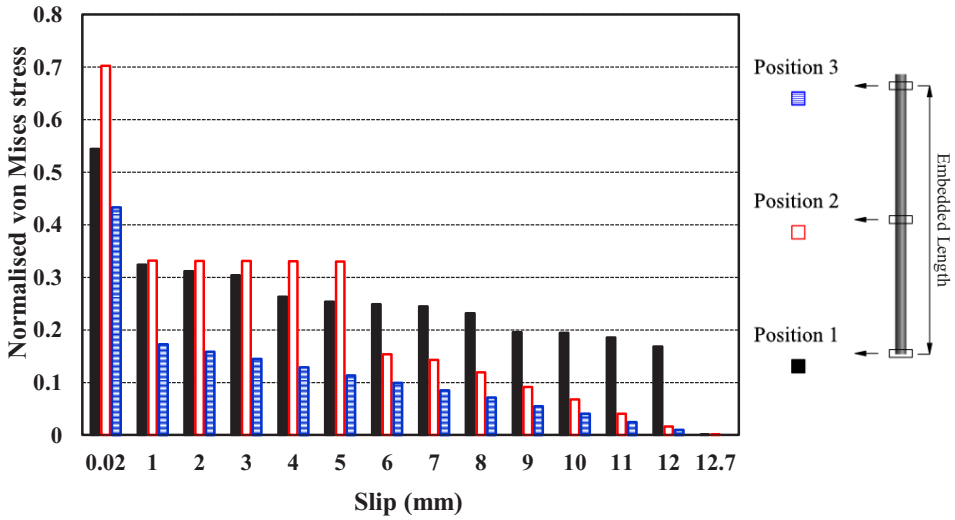

Fig. 11. Normalised von Mises stress versus slip of the straight fibre.

It is well known that straight steel fibres are normally characterised by linear bond-slip softening behaviour after the fibre-matrix interface debonding which implies a constant shear stress at the interface [7]. The bond strength of such fibres embedded in concrete is generally small and mostly frictional in nature [17]. However, by tailoring the matrix composition and surface coating of the fibres, it is possible to achieve slip-hardening behaviour. The key feature of such performance is that when the fibre is pulled out from the matrix, its resistance increases with the slippage. This is attributed to the intensive damage of the fibre surface by matrix particles during the pullout process leading to increase in the interface friction and consequent improvement in bond behaviour [4,16]. Hence, during pullout depending on the interface properties, matrix composition, and the fibre shape, the coefficient of friction at the interface could increase.

4.2. HOOKED-END STEEL FIBRE

In this section, a hooked-end steel fibre pullout, performed by Jamee [31] is investigated. The geometrical properties of the fibre are shown in **Fig. 12**. The yield and ultimate stresses (f_y and f_u) of the fibre material are 650 MPa and 800 MPa, and the cylinder compressive strength and the elastic modulus of the cementitious matrix (f_{ck} and E_c) are 60 MPa and 38 GPa, respectively. Using **Eq. (1)** the mean tensile strength of concrete is estimated to be 4.6 MPa.

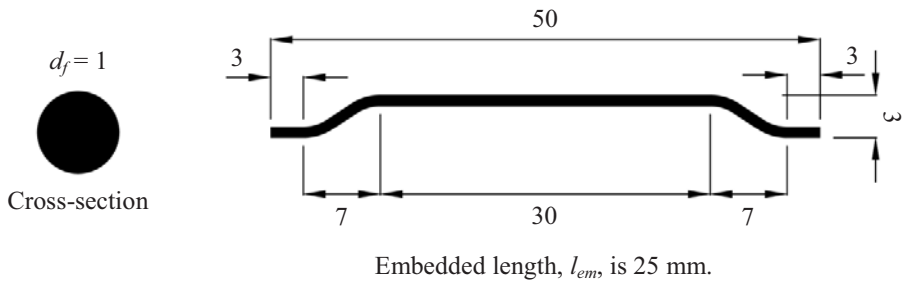

Fig. 12. Dimensions of the hooked-end steel fibre (in mm).

Fig. 13 shows the FE model of the hooked-end fibre embedded in the matrix. As seen in the figure, half of the specimen is modelled because of the symmetry. The contact parameters used for this model are presented in **Table 2**.

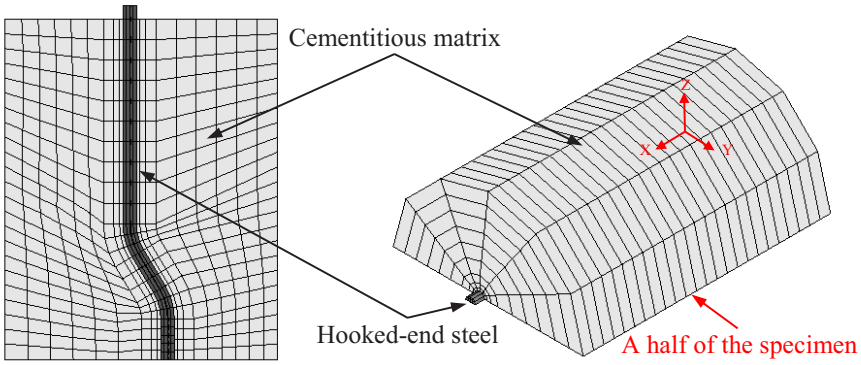

Fig. 13. Finite element model of the hooked-end fibre.

The bond-slip curves of the numerical model and the experimental specimen are represented in **Fig. 14** in which good agreement is observed; in particular, the model properly captures the two expected load drops during the pullout process.

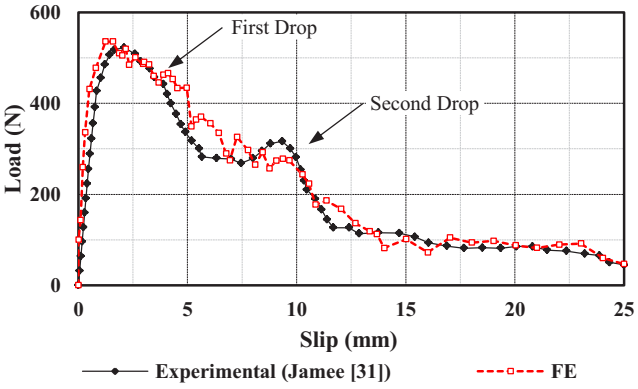

Fig. 14. Experimental and numerical load-slip curves of the hooked-end fibre.

In **Fig. 15**, the von Mises stress contours of the fibre at slips equal 0.45 mm and 2 mm which correspond to the complete interface debonding and the initiation of the first drop in the load-slip curve (see **Fig. 14**) are illustrated. As seen in the figure, as a result of the fibre tendency to change its shape during passing through the two curved regions of the matrix, i.e. fibre straightening, plastic hinges are formed in the fibre in the vicinity of those regions.

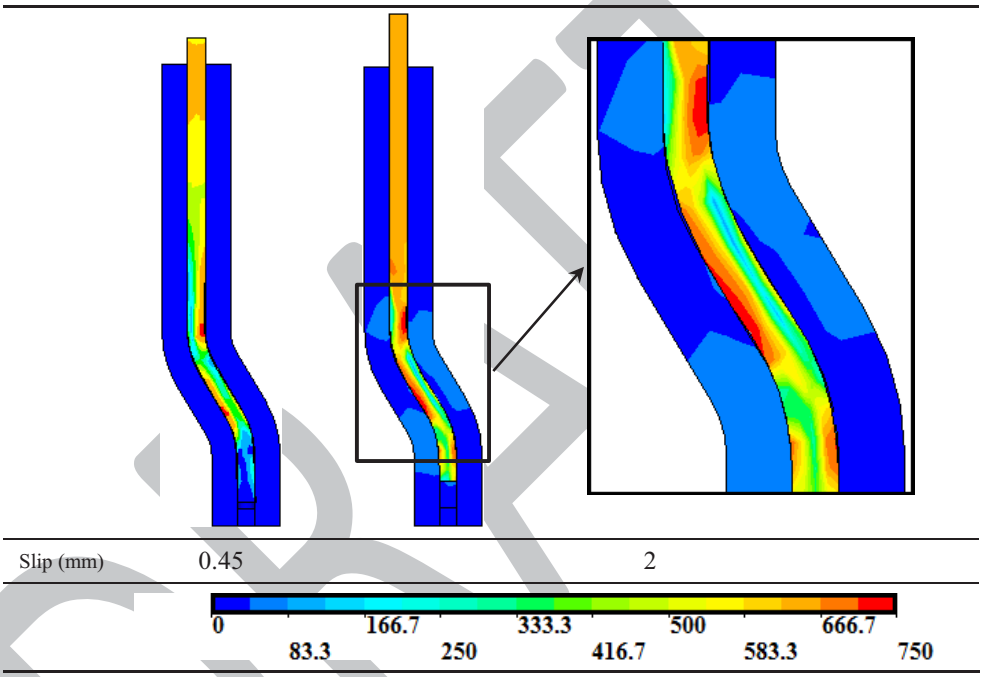

Fig. 15. The von Mises stress contours (in MPa) of the hooked-end fibre.

Average interfacial shear stress versus slip is shown in **Fig. 16**. The graph consists of three distinctive parts, a steep initial ascending portion, followed by a smoothly descending branch up to the slip equals 12.5 mm and then an ascending branch up to the complete fibre withdrawal. As observed in **Fig. 14**, after slip around 12.5 mm, even though the interface is decreasing, there is only marginal load decay which leads to the continuous increase of the average interfacial shear stress after this slip, as seen in **Fig. 16**. It is attributed to the incomplete straightening of the fibre

and existing permanent deformations at the fibre end where the fibre experiences higher levels of frictional stress compared with the other interface areas (see **Figs. 17(a)** and **(b)**).

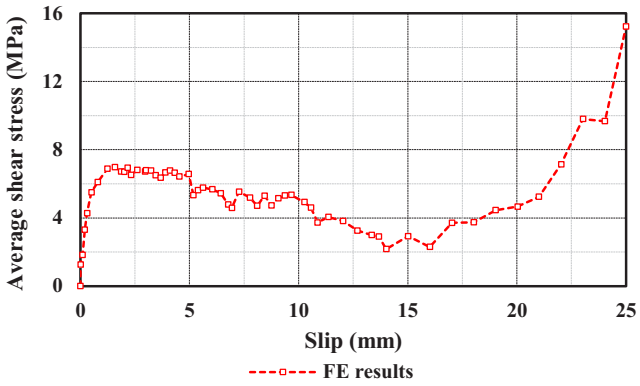

Fig. 16. Average interfacial shear stress versus slip for the hooked-end fibre.

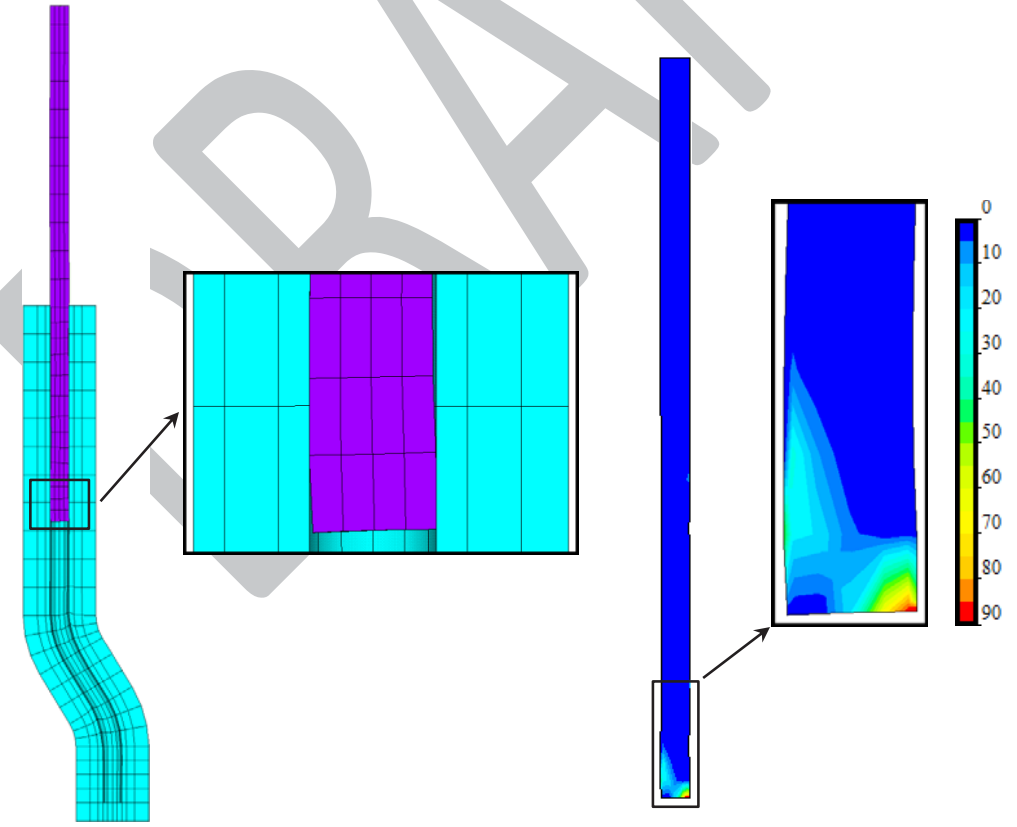

(a) Permanent deformation **(b)** Interfacial shear stress (in MPa)

Fig. 17. Pullout mechanism after straightening of the end hook, slip = 16.5 mm.

The normalised von Mises stress at three cross-sections located at the bottom and top of the fibre as well as the middle of the end hook are plotted versus displacement in **Fig. 18**. Regarding the bottom level, as it is observed, there are two peak points, each one followed by a trough point, as a result of fibre straightening, and then relatively high levels of stress compared with the two other regions. These levels of stress are indicative of the dominant contribution of the fibre end to the pullout load (see **Fig. 17(b)**).

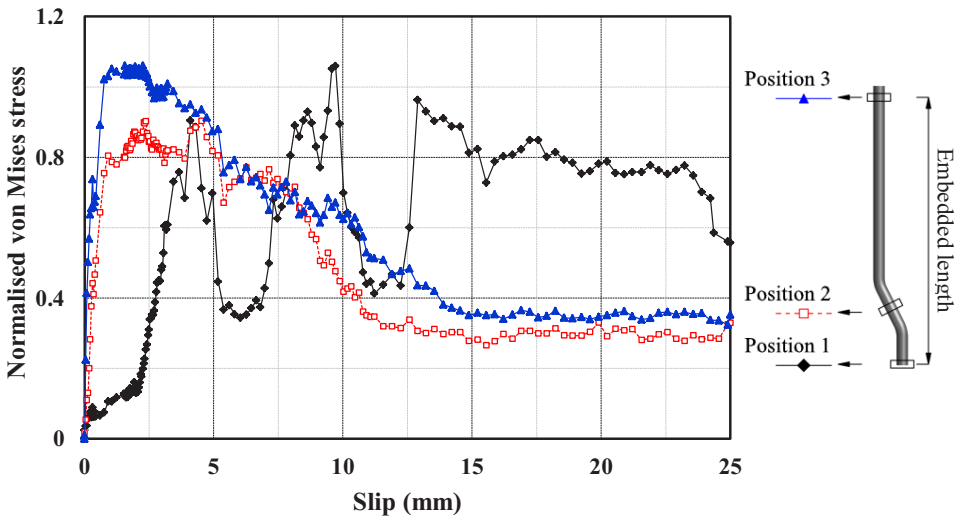

Fig. 18. Normalised von Mises stress versus displacement of the hooked-end fibre.

4.3. CRIMPED STEEL FIBRE

Pullout testing data of a crimped steel fibre with an embedded length of 15 mm [8] are employed for further validation. The geometrical properties of the fibre are shown in **Fig. 19**.

The yield and ultimate stresses of the fibre material are 1450 MPa and 1800 MPa, respectively and the cylinder compressive strength of the cementitious matrix is 39 MPa. The mean tensile

strength and Young's modulus of the matrix are estimated to be 3.5 MPa and 35 GPa, respectively. The adjusted contact parameters for the model are provided in **Table 2**.

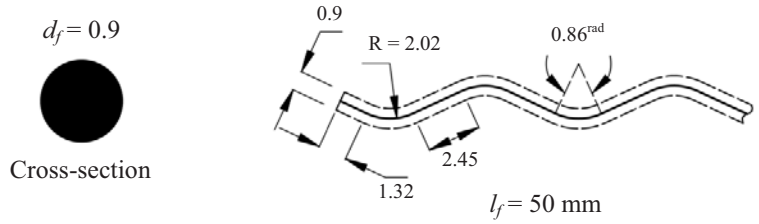

Fig. 19. Geometrical properties of the crimped steel fibre (in mm).

Fig. 20 shows the comparison of the experimental and numerical bond-slip curves where good agreement is found and the model can reasonably predict the bond-slip behaviour of the fibre throughout the pullout process.

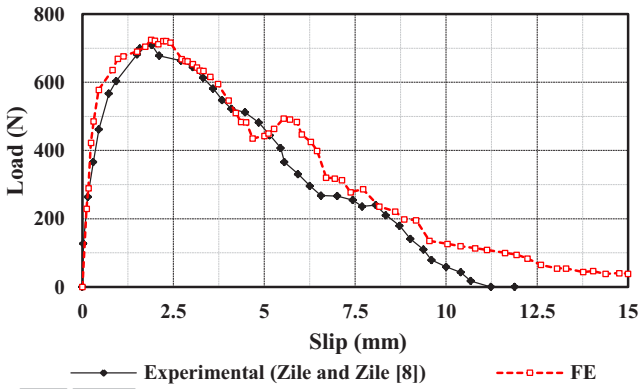

Fig. 20. Experimental and numerical load-slip curves of the crimped fibre.

Fig. 21 shows the von Mises stress contour of the fibre at a slip equal to 0.3 mm, which corresponds to the complete interface debonding.

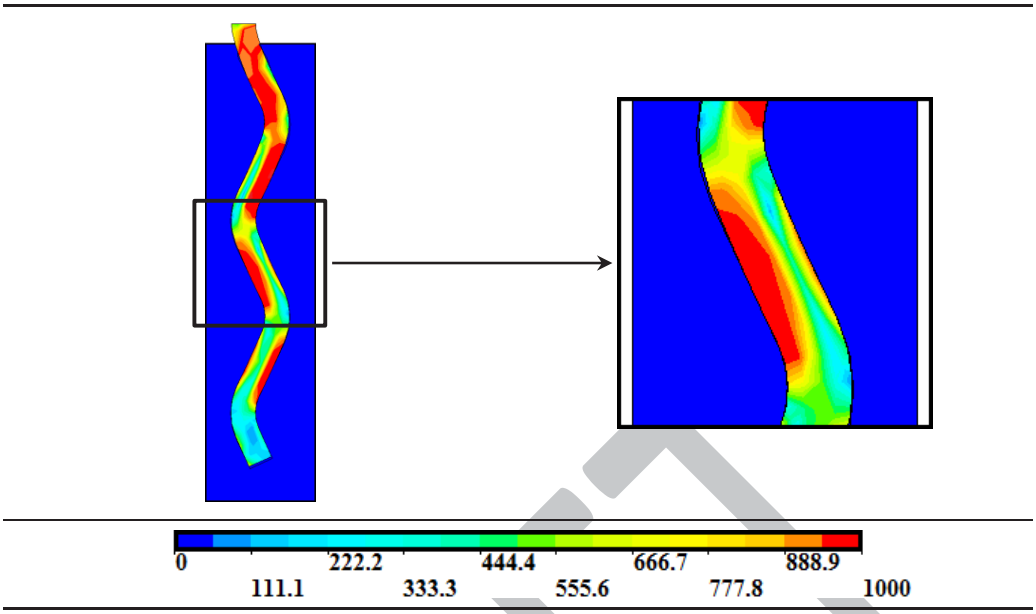

Fig. 21. The von Mises stress contour (in MPa) of the crimped fibre at slip = 0.3 mm.

The normalised von Mises stress with respect to the yield stress at three levels, bottom, middle and top of the fibre versus displacement is shown in **Fig. 22**. The results indicate that during pullout, the embedded length of the fibre is subjected to repetitive bending and straightening, which result in improving the interface friction and consequently increase in the pullout load.

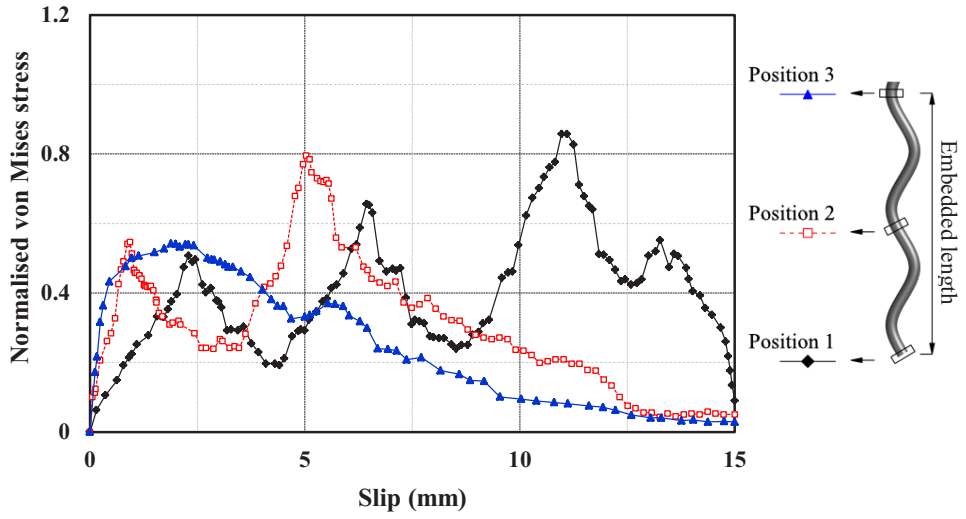

Fig. 22. Normalised von Mises stress versus displacement of the crimped fibre.

4.4. TWISTED STEEL FIBRE

The pullout performance of steel fibres directly depends on the physicochemical bond and mechanical anchorage. While mechanical anchorage just depends on the fibre geometry, physicochemical bond relies upon the collaborative contribution of the fibre-matrix interface, matrix packing density, and the fibre geometry [4,43,44]. Just after full debonding and initiation of slippage, depending on the fibre-matrix interface, matrix packing density and the fibre shape, the fibre surface experiences continuous damage, scratching, and delamination which leads to gradual increase in the interfacial friction [4,17]. However, in most cases the combined effect of the aforementioned factors just results in a marginal increase of the interfacial friction. The commercially-available twisted fibres are engineered in terms of shape, size, and mechanical properties, as well as compatibility with a given matrix to achieve higher rates of increase in the interface friction, i.e. slip hardening behaviour [17].

In this section, as the final step for validation of the proposed numerical model, a rectangular twisted fibre embedded in ultra-high performance concrete tested by Wille and Naaman [4] is employed in which the fibre shows slip hardening behaviour. The total and embedded lengths of the fibre are 13 mm and 6.5 mm, respectively and the cross-sectional dimensions are 0.24 mm by 0.3 mm. Moreover, the fibre pitch, i.e., the length of one full (360-degree) twist around the fibre axis, is 8 mm. The yield and ultimate stresses of the fibre material are 3100 MPa and 3400 MPa, respectively and the cylinder compressive strength of the cementitious matrix is 100 MPa. Since the actual values of the mean tensile strength and Young's modulus of the matrix were not reported, they are estimated to be 6.5 MPa and 44 GPa, using **Eqs. (1)** and **(2)**.

The contact parameters for the model are provided in **Table 2**. The dynamic coefficient of friction is assumed to be linearly correlated to the fibre slip, according to **Eq. (9)**.

$$\mu_d = 0.037\upsilon + 0.44 \quad (9)$$

In **Fig. 23** and **Fig. 24**, the experimental and numerical pullout load and interfacial shear stress curves, both versus slip are provided where reasonable correlations are achieved. **Fig. 25** shows the von Mises stress contours of the fibre at slips equal 0.015 mm, 1.35 mm, and 6 mm which respectively correspond to the debonding load, the peak load, and the complete pullout from the matrix.

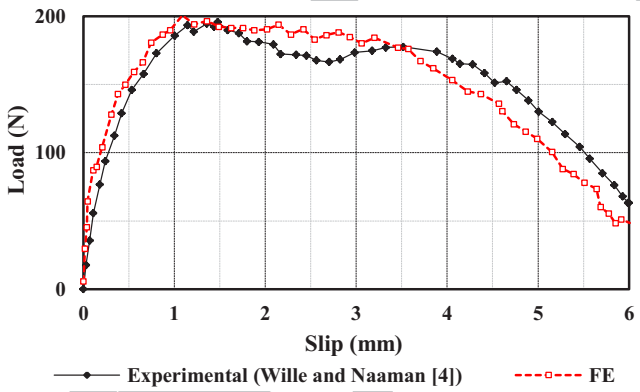

Fig. 23. Experimental and numerical load-slip curves of the twisted fibre.

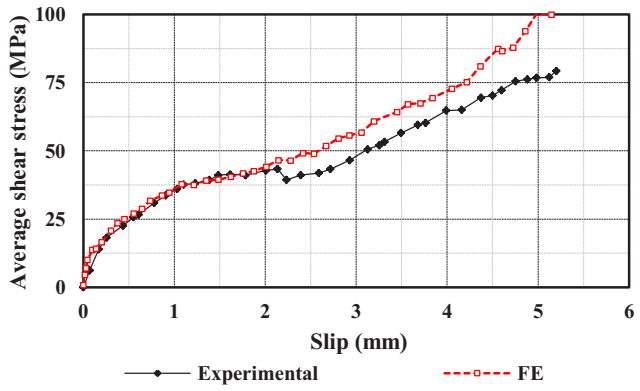

Fig. 24. Average interfacial shear stress versus slip for the twisted fibre.

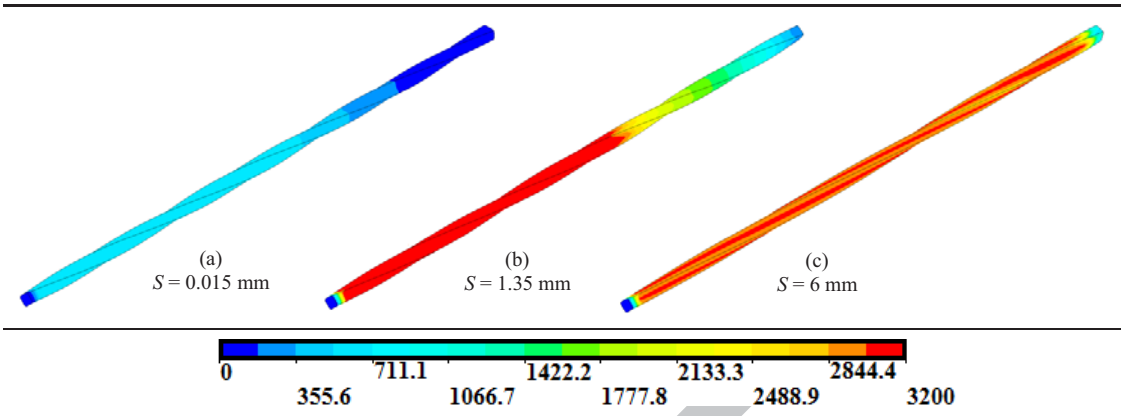

Fig. 25. The von Mises stress contours (in MPa) of the twisted fibre at slips correspond to **(a)** debonding load, **(b)** peak load, and **(c)** the complete pullout.

In addition, the normalised von Mises stress at five levels along the fibre length, 0.5 mm, 2 mm, 3 mm, 4 mm, and 6 mm from the bottom of the fibre is plotted versus displacement in **Fig. 26**. The results are indicative of the effectiveness of the twist (as the mechanical anchorage) along the fibre which leads to higher performance and favourable stress distribution along the fibre.

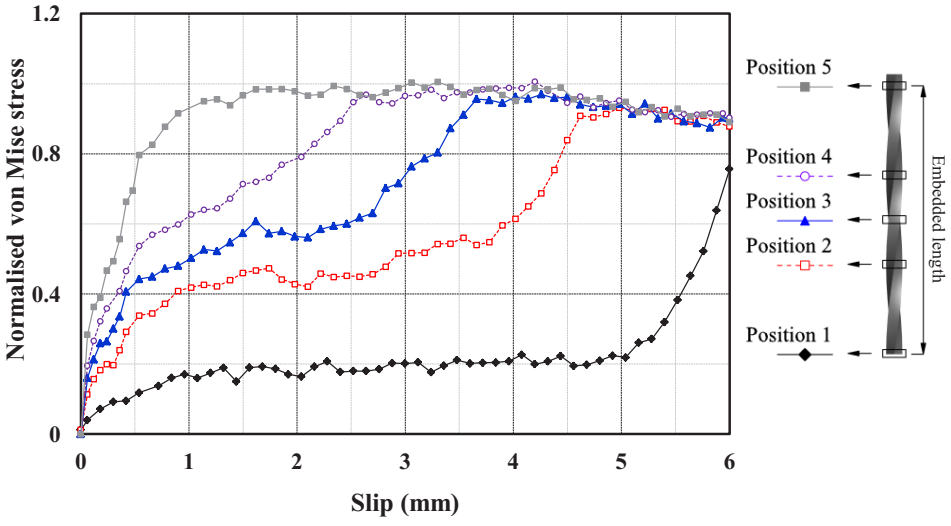

Fig. 26. Normalised von Mises stress versus displacement at five levels of the twisted fibre.

5. PULLOUT SIMULATION OF FIBRES WITH NEW GEOMETRIES

In this section, the validated numerical model is employed as a virtual laboratory unit to investigate the pullout performance of two steel fibres with new shapes (NF-1 and NF-2) where the hooked-end fibre validated in **Section 4.2** is considered as the basis of their geometry. Two new steel fibres with two hooks at each end but with different configurations are developed, as seen in **Fig. 27**.

Fibre ID	Configuration	Cross-section
NF-1	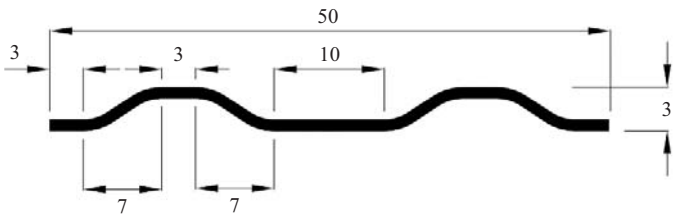	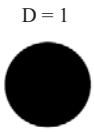
NF-2	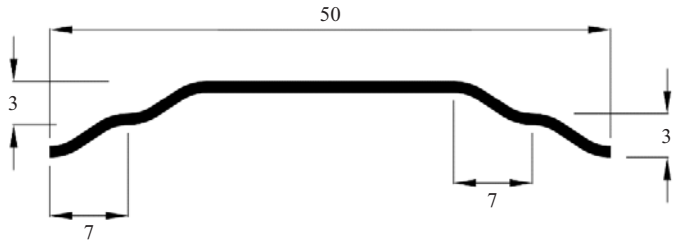	
Embedded length, l_{em}, is 25 mm.		

Fig. 27. Dimensions of the new steel fibres (in mm).

It was also assumed that the surface roughness of steel and concrete materials and also the concrete strength are the same as those of the hooked-end model. Therefore, the contact parameters of the new fibres' models are considered to be the same as those of the hooked-end model. In general, the contact parameters (especially coefficients of friction and cohesion) mostly affect the magnitude of the pullout loads not the overall trend of the pullout load-slip

curve. It is worth mentioning that in the development process of any new steel fibres, if the preliminary FE pullout results indicate that the fibre possesses favourable pullout characteristics (irrespective of the magnitude of the pullout load), experimental pullout tests are required to adjust the contact parameters and re-validate the numerical model.

Since the new fibres benefit from stronger (heavier) mechanical anchorages compared with the hooked-end fibre, during pullout process the fibres fractured. A few simulations are performed to optimise the fibres materials, so that the complete fibres withdrawal is achieved. The optimised yield and ultimate stresses of steel material for NF-1 and NF-2 fibres are found to be 1600 MPa and 2000 MPa, and 1000 MPa, and 1250 MPa respectively.

The pullout load-slip curves of the new fibres and the hooked-end fibre are illustrated in **Fig. 28**.

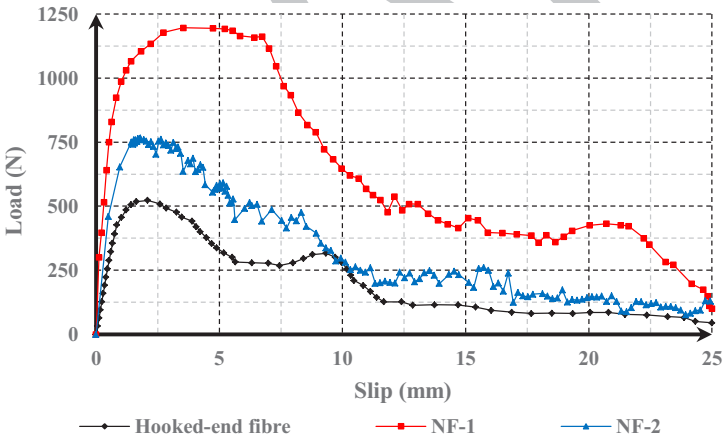

Fig. 28. The load-slip curves of the hooked-end and the two new fibres.

From the graph, it is evident that the double-hook enhances the bond-slip response of the fibres. The comparison of the maximum pullout load (P_{max}) and total dissipated pullout energy (E_t) of the new and ordinary hooked-end steel fibres are provided in **Table 3**. In **Fig. 29**, the von Mises stress contour of the new fibres at varying slips is shown. As seen, high levels of stress are

developed in the fibres in the vicinity of the curved regions of the matrix. During the pullout process, the curved parts of the fibre (the mechanical anchorages) have the main contribution to the pullout resistance.

Table 3
Pullout results of the hooked-end and two new steel fibres.

Fibre Type	Label	P_{max} (N)	Improvement (%)	E_t (N.m)	Improvement (%)
Hooked-end	1	522.60	-	5.07	-
NF-1	2	1195.92	128.7%	16.29	2.2%
NF-2	3	766.01	46.6%	6.79	33.9%

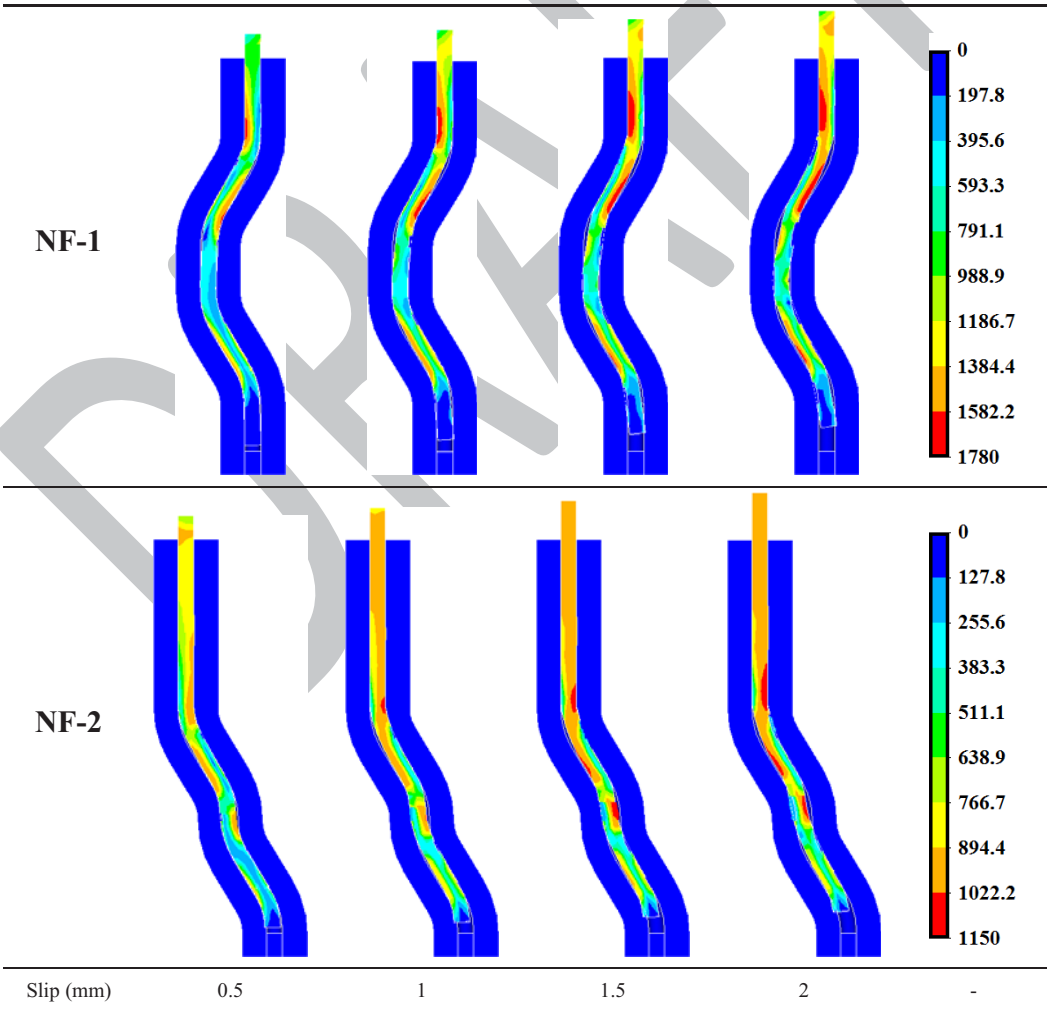

Fig. 29. The von Mises stress contour (in MPa) of the new steel fibres at varying slips.

Overall, NF-1 and NF-2 fibres have relatively higher efficiencies compared with the hooked-end fibre; however, they suffer from significant pullout load decay following the peak load as the hooked-end fibre.

6. REMARKS

This paper presents a generic nonlinear finite element model to simulate the bond-slip behaviour of steel fibre in concrete matrix. The following conclusions can be drawn:

1) In the numerical FE model, contact elements are employed to simulate the fibre-matrix interaction in which the Coulomb friction model is introduced to consider physicochemical bond and the fibre-matrix interface friction. In addition, geometric and material nonlinearity are considered in the model. The findings of this research verify the accuracy of the numerical model to simulate the steel fibre pullout mechanism, where good agreement between the experimental and numerical results is achieved. Moreover, the details which could be obtained from the simulations are significantly higher than those of the tests.

2) The conventional fibre development approach is a repetitive process including fibre design, manufacturing and experimental testing which are time consuming and not cost effective. In the future, designing and optimisation of new types of steel fibre could be done with the help of the proposed numerical model which will considerably decrease the number of experiments and corresponding costs.

3) It should be noted that in real scenarios, the cracks might initiate at any point along the fibre and the fibre generally slips on the shorter embedded side. This could highly affect the pullout performance of steel fibres especially those which are fully deformed such as crimped and twisted. Therefore, pullout study should be performed on fibres with various embedded lengths and angles of inclinations.

REFERENCE

[1] Brandt AM. Fibre reinforced cement-based (FRC) composites after over 40 years of development in building and civil engineering. Compos Struct 2008;86:3-9.

[2] Abbass W, Khan MI, Mourad S. Evaluation of mechanical properties of steel fiber reinforced concrete with different strengths of concrete. Constr Build Mater 2018;70:243-253.

[3] Banthia N, Trottier JF. Concrete reinforced with deformed steel fibers, part I: Bond-slip mechanisms. ACI Mater J 1994;91-M43:435-446.

[4] Wille K, Naaman AE. Pullout behavior of high-strength steel fibers embedded in ultra high performance concrete. ACI Mater J 2012;109-M46:479-488.

[5] Carnovale DJ. Behaviour and analysis of steel and macro-synthetic fibre reinforced concrete subjected to reversed cyclic loading: A pilot investigation. Master of applied science thesis, University of Toronto, Ontario, Canada, 2013.

[6] Naaman AE, Najm H. Bond-slip mechanisms of steel fibers in concrete. ACI Mater J 1991;88-M17:135-145.

[7] Naaman AE, Namur GG, Ahvan JM, Najm HS. Fiber pullout and bond slip. II: Experimental validation. J Struct Eng-ASCE 1991;117:2791-2800.

[8] Kim DJ, Naaman AE, El-Tawil S. High performance fiber reinforced cement composites with innovative slip hardending twisted steel fibers. Int J Concr Struct Mater 2009;3:119-126.

[9] Zīle E, Zīle O. Effect of the fiber geometry on the pullout response of mechanically deformed steel fibers. Cement Concrete Res 2013;44:18-24.

[10] Chao SH, Cho JS, Karki NB, Sahoo DR, Yazdani N. FRC performance comparison: uniaxial direct tensile test, third-point bending test, and round panel test. ACI Special Publication 2011;276:1-20.

[11] Armelin SH, Banthia N. Predicting the flexural postcracking performance of steel fiber reinforced concrete from the pullout of single fibers. ACI Mater J 1997;94(1):18-31.

[12] Prudencio L, Austin S, Jones P, Armelin H, Robins P. Prediction of steel fibre reinforced concrete under flexure from an inferred fibre pullout response. Mater Struct 2006;39(6):601-610.

[13] Mobasher B, Bakhshi M, Barsby C. Backcalculation of residual tensile strength of regular and high performance fiber reinforced concrete from flexural tests. Constr Build Mater 2014;70:243-253.

[14] Soranakom C, Mobasher B. Closed-form solutions for flexural response of fiber-reinforced concrete beams. J Eng Mech-ASCE 2007;133(8):931-941.

[15] Soranakom C, Mobasher B. Closed-form moment-curvature expressions for homogenized fiber-reinforced concrete. ACI Mater J 2007;104-M39:351-359.

[16] Wille K, Naaman AE. Effect of ultra-high-performance concrete on pullout behavior of high-strength brass-coated straight steel fibers. ACI Mater J 2013;110-M41:451-462.

[17] Naaman AE. Engineered steel fibers with optimal properties for reinforcement of cement composites. J Adv Concr Technol 2003;1:241-252.

[18] Naaman AE, Namur GG, Alwan JM, Najm HS. Fiber pullout and bond slip. I: Analytical study. J Struct Eng-ASCE 1991;117:2769-2790.

[19] Laranjeira F, Molins C, Aguado A. Predicting the pullout response of inclined hooked steel fibers. Cement Concrete Res 2010;40:1471-1487.

[20] Van Gysel A. Studie van het uittrekgedrag van staalvezels ingebed in een cementgebonden matrix met toepassing op staalvezelbeton onderworpen aan buiging (in Dutch). PhD thesis, Gent University, Belgium, 2000.

[21] Soetens T, Van Gysel A, Matthys S, Taerwe L. A semi-analytical model to predict the pullout behaviour of inclined hooked-end steel fibres. Constr Build Mater 2013;43:253-265.

[22] Alwan JM, Naaman AE, Guerrero P. Effect of mechanical clamping on the pullout response of hooked steel fibers embedded in cementitious matrices. Concr Sci Eng 1999;1:15-25.

[23] Sujivorakul C, Waas AM, Naaman AE. Pullout response of a smooth fiber with an end anchorage. J Eng Mech 2000;126 (9):986-993.

[24] Laranjeira F, Aguado A, Molins C. Predicting the pullout response of inclined straight steel fibers. Mater Struct 2010;43:875-895.

[25] Laranjeira F, Molins C, Aguado A. Predicting the pullout response of inclined hooked steel fibers. Cement Concrete Res 2010;40(10):1471-1487.

[26] Tsai JH, Patra A, Wetherhold R. Finite element simulation of shaped ductile fiber pullout using a mixed cohesive zone/friction interface model. Compos Part A-Appl S 2005;36:827-838.

[27] Li CY, Mobasher B. Finite element simulations of fiber pullout toughening in fiber reinforced cement based composites. Adv Cem Based Mater 1998;7:123-132.

[28] Yang QS, Qin QH, Peng XR. Size effects in the fiber pullout test. Compos Struct 2003;61:193-198.

[29] Georgiadi-Stefanidi K, Mistakidis E, Pantousa D, Zygomalas M. Numerical modelling of the pull-out of hooked steel fibres from high-strength cementitious matrix, supplemented by experimental results. Constr Build Mater 2010;24:2489-2506.

[30] Chin CS, Xiao, RY. Experimental and Nonlinear Finite Element Analysis of Fiber Cementitious Matrix Bond-Slip Mechanism, in High Performance Fiber Reinforced Cement Composites 6; Parra-Montesinos G, Reinhardt H, Naaman, AE, editors; Springer 2012.

[31] Jamee M. Effect of hooked-end fibers pull-out behavior on the mechanical properties of fiber reinforced concrete. Master's thesis, Shahrood University of Technology, Iran, 2013.

[32] ANSYS®. Academic Research, Release 16.1. Canonsburg (PA, USA): ANSYS Inc.; 2015.

[33] Willam KJ, Warnke EP. Constitutive models for the triaxial behavior of concrete, in Proceedings of the international assoc. for bridge and structural engineering. Bergamo (Italy) 1975;1-30.

[34] Eurocode 2: Design of concrete structures, Part 1-1: General rules and rules for buildings; 2004.

[35] Wriggers P, Vu Van T, Stein E. Finite element formulation of large deformation impact contact problems with friction. Comput Struct 1990;37:319-331.

[36] Hallquist JO. LS-DYNA theoretical manual. Livermore Software Technology Corporation; 1998.

[37] Bathe KJ. Finite element procedures. Englewood Cliffs, New Jersey: Prentice-Hall; 1996.

[38] Cook RD, Malkus DS, Plesha ME. Concept and applications of finite element analysis (3rd edition). New York: John Wiley; 1989.

[39] Gu RJ, Murty P, Zheng Q. Use of penalty variable in finite element analysis of contacting objects. Comput Struct 2002;80:2449-2459.

[40] Weyler R, Oliver J, Sain T, Cante JC. On the contact domain method: A comparison of penalty and Lagrange multiplier implementations. Comput Method Appl M 2012;205-208:68-82.

[41] Belytschko T, Yeh IS. The splitting pinball method for contact-impact problems. Comput Method Appl M 1993;105:375-393.

[42] Laursen TA, Simo JC. Algorithmic symmetrization of coulomb frictional problems using augmented lagrangians. Comput Method Appl M 1993;108:133-146.

[43] Abbass W, Khan MI. Fiber-Matrix Interactions in Fiber-Reinforced Concrete: A Review. Arab J Sci Eng 2016;41(4):1183-1198.

[44] Abdallah S, Fan M, Zhou X, Le Geyt S. Anchorage Effects of Various Steel Fibre Architectures for Concrete Reinforcement. Int J Concr Struct M 2016;10(3):325-335.